Efficient laser emission from cladding waveguide inscribed in Nd:$GdVO_4$ crystal by direct femtosecond laser writing

Hongliang Liu,[1] Yang Tan,[1] Javier R. Vázquez de Aldana,[2] and Feng Chen[1,*]

[1]*School of Physics, State Key Laboratory of Crystal Materials, Shandong University, Jinan 250100, China*

[2]*Laser Microprocessing Group, Universidad de Salamanca, Salamanca 37008, Spain*

**Corresponding author: drfchen@sdu.edu.cn*

Received April 1, 2014; revised June 24, 2014; accepted June 29, 2014;
posted July 1, 2014 (Doc. ID 209282); published July 29, 2014

We report on the fabrication of depressed cladding waveguides in Nd:$GdVO_4$ laser crystal by using femtosecond laser inscription. The cross section of the structure is a circular shape with a diameter of 150 μm. Under the optical pump at 808 nm, the continuous wave (cw) as well as pulsed (*Q*-switched by graphene saturable absorber) waveguide lasing at 1064 nm has been realized, supporting guidance of both TE and TM polarizations. The maximum output power of 0.57 W was obtained in the cw regime, while the maximum pulse energy of the pulsed laser emissions was up to 19 nJ (corresponding to a maximum average output power of 0.33 W, at a resonant frequency of 18 MHz). The slope efficiencies achieved for the cw and pulsed Nd:$GdVO_4$ waveguide lasers were as high as 68% and 52%, respectively.

OCIS codes: (230.7370) Waveguides; (140.3390) Laser materials processing; (130.3120) Integrated optics devices.
http://dx.doi.org/10.1364/OL.39.004553

Neodymium doped gadolinium vanadate (hereafter Nd:$GdVO_4$) is one of the well-known gain media for laser diode (LD) pumped solid state laser systems. Because of its higher thermal conductivity, higher damage thresholds, and larger emission cross section, particularly the higher pump absorption coefficient (33.2 cm^{-1} at 808 nm) compared to the Nd:YAG (9.1 cm^{-1} at 808 nm) or Nd:GGG (14.5 cm^{-1} at 808 nm) gain media, Nd:$GdVO_4$ crystal has great application for the development of solid state lasers [1–3]. Femtosecond (fs) laser writing has been utilized to fabricate waveguides in transparent materials since the pioneer work from Davis *et al.* [4]. The refractive indices of the materials are either negatively or positively changed along the inscribed tracks because of the induced effects from the stress fields and the lattice damages [5]. Focused at a spot and producing a heat-affected zone both in micrometric or sub-micrometric scales, the fs laser inscribed waveguides preserve the fluorescence properties of the doped-rare ions well in the waveguide area. Benefiting from the large pump area and isotropic induced-stress field, depressed cladding waveguides (also called Type III configuration, typically located in a core surrounded by a number of low-index fs-laser written filaments) support waveguide lasers at both TM and TE polarizations with excellent waveguide laser performance [5]. Typically, the step-by-step translation technique is often used for fabricating cladding waveguides, which was first proposed by Okhrimchuk *et al.* and applied in Nd:YAG crystals in 2005 [6]. Diverse configurations of depressed cladding waveguides—were produced in crystalline dielectric materials (e.g., Nd:LGS [7], BiB_3O_6 [8]), Nd:YAG ceramics and crystals [9,10], Tm^{3+}:ZBLAN [11], and Cr:ZnSe [12].

Waveguide lasers are miniature light sources, which have significant applications in integrated photonics [13]. Different from cw lasers, the pulsed lasers play a more important role in a number of photonic applications, such as frequency comb generation, nonlinear microscopy and medicine optics [14–25]. With appropriate saturable absorbers, e.g., semiconductor saturable absorber mirror (SESAM) [14], semiconductor quantum dots (QDs) materials (PbS QD glass) [15], sing-wall carbon nanotube (SWCNT) [16], and graphene [17], pulse lasers have been achieved in numerous systems. The passive *Q*-switched mode-locked laser was first obtained in Nd^{3+}-doped glass rods in 1966 [18]. In waveguides, lasers have been passively *Q*-switched or modelocked in transparent materials (i.e., Nd:YAG crystal [19], Nd-doped glass [20], Yb:KYW [21], Yb:YAG [22], and Ti:Er:$LiNbO_3$ [23]). Recently, the graphene saturable absorber (GSA) offers great potential for applications because of its relatively low saturation absorption intensity, large modulation depth, and sufficient saturable absorption over an ultrabroad range of wavelengths, compared with a wavelength range of 800–2070 nm for SWCNT [17,18,24].

In this Letter, we report on the fabrication of Nd:$GdVO_4$ circular cladding waveguides inscribed with multiple fs-laser damage tracks. The cw waveguide laser oscillation at 1.06 μm was generated using an optical pump at 808 nm. Furthermore, by using bilayer GSA on quartz, a passively *Q*-switched pulse waveguide laser was achieved for both TE and TM polarizations.

The *a*-cut Nd:$GdVO_4$ crystal sample (doped by 2 at. % Nd^{3+} ions) was cut with sizes of 2 mm×3.7 mm×8 mm along *a*, *b* and *c* axes, respectively. The circular depressed cladding waveguides were produced by using the laser facility of the Universidad de Salamanca, Spain, in which a Ti:Sapphire regenerative amplifier (Spitfire, Spectra Physics, USA) was used as a laser source for the experimental setup shown in Fig. 1(a). It delivered linearly polarized pulses of 120 fs and 795 nm central wavelength at a 1 kHz repetition rate as reported in previous works [7,8]. The maximum available pulse energy was 1 mJ, and it was reduced with a calibrated neutral density filter placed after a half-wave plate and a linear polarizer to get a fine control of the incident energy.

A depressive cladding waveguide (with a cross-sectional diameter of 150 μm) was inscribed inside the

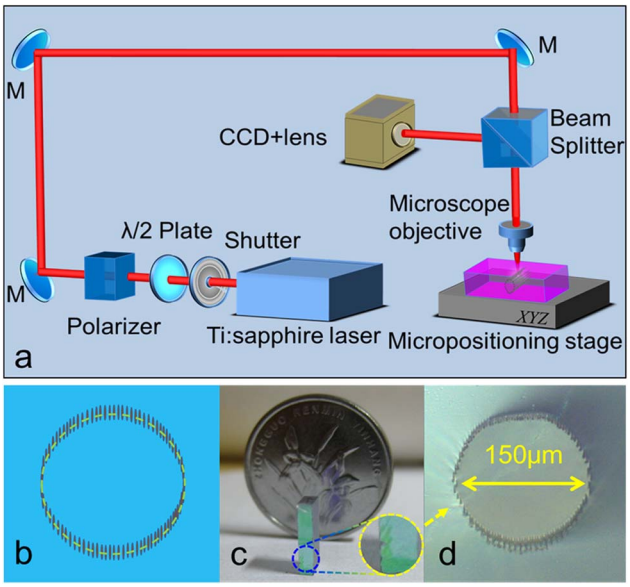

Fig. 1. (a) Experimental setup of the fs-laser inscription process of depressed cladding waveguides in Nd:$GdVO_4$ crystal, (b) cross-sectional design of cladding waveguides, (c) photograph of the sample with the end face coated by a thin film (the inset is the enlarged photograph of the waveguides), and (d) microscopic cross-sectional image of the cladding waveguide with a diameter of 150 μm.

Nd:$GdVO_4$ crystal. The center was ~225 μm below the surface. During the fabrication process of the cladding waveguides, the pulse energy was set to 1.68 μJ and the laser beam was focused with a 40× microscope objective (N.A. ~0.65). The sample was scanned at a constant velocity of 500 μm/s in the direction parallel to the 3.7 mm edge, thus producing a damage line along the sample. The procedure was repeated at different depths of the sample, following the desired circular geometry with a lateral separation of 3 μm between each two adjacent tracks as shown in Fig. 1(b). Figure 1(c) is a photograph of the sample with the end face coated by a thin film, and the inset image shows an enlargement of the waveguide area in which the waveguides could be roughly watched. The thin film (high reflectivity at 1.06 μm and high transmission at 808 nm) was coated on the input surface of Nd:$GdVO_4$ and acted as the resonator high-reflectivity mirror (HRM). Under these conditions, a tubular-shape structure with a diameter of 150 μm was fabricated [see Fig. 1(d)] for the cross sectional images of the waveguide with a diameter of 150 μm). Some cracks at the surroundings of the waveguides are observed at this irradiation conditions because of the large stress induced in the crystal, but they do not affect the waveguide core.

With the measurement of the N. A. of the waveguides and using the formula reported in [25], we obtained the maximum change of refractive index $\Delta n \approx 2.0\times10^{-3}$ of the waveguide. In spite of the method itself being a rough estimation, this value was in good agreement with those reported for other cladding waveguides [7–11] fabricated under analogous irradiation conditions. The back-reflection method [26] was used to measure the losses of the cladding waveguides at 632.8 nm with a He–Ne laser as a light source. The measured values for TM modes were as low as ~0.7 dB/cm, which was lower than those measured for TE modes, and the losses of the bulk substrate were about 0.65 dB/cm. Nevertheless, the difference of losses between TE and TM polarized modes was within 10%.

A tunable cw Ti:Sapphire laser (Coherent MBR 110, USA) which generated a linearly polarized beam at 808 nm was used in the end pumping system to perform the cw and passively Q-switched waveguide laser operation experiments at room temperature. A spherical convex lens with a focal length of 75 mm was used to couple the pump laser beam into the waveguide, and a 20× microscope objective lens (N.A. = 0.4) was used to collect the generated waveguide laser light and to image it on an IR CCD camera through an aperture. A spectrometer and an oscilloscope (Tektronix TDS 202 2B, 200 MHz) were used to analyze the emission spectra and pulse trains of the generated waveguide laser beams.

We calculated the output powers for the cw output power versus the launched pump power, taking into account the transmittance and reflectivity of the optical elements (e.g., microscope lenses) in the end-coupling experiment. Results are shown in Fig. 2. The maximum output powers measured were $P_{\mathrm{max,cw}} \approx 0.57$ W. From the linear fit of the experimental data we obtained the thresholds of the cw waveguide laser $P_{\mathrm{th,cw}} \approx 178$ mW. In addition, the extracted slope efficiency of the laser is $\eta_{\mathrm{cw}} \approx 68\%$. In fact, the slope efficiency of 68% is quite close to the quantum defect limit between the pump and laser photons (~76%). Compared with our previous work [27], the slope efficiency 68% of the cladding waveguide in Nd:$GdVO_4$ system was almost the same as that of the fs-laser written double-line waveguide (~70%). In addition, the maximum output power of 0.57 W in this work has increased by ~120% as compared with the double-line structure (256 mW), which was a considerable enhancement of the laser performance. The optical-to-optical efficiency at the maximum output power of 0.57 W was calculated to be 63%.

For the Q-switched pulsed laser-operation experiment, the bilayer graphene deposited on quartz was utilized as the saturable absorber as depicted in Fig. 3(a). The bilayer graphene coated on quartz was provided by Hefei Vigon Material Technology Co., Ltd, China. The transmission of the GSA (bilayer graphene coated on circular quartz plate) was measured to be 92% at 1064 nm It

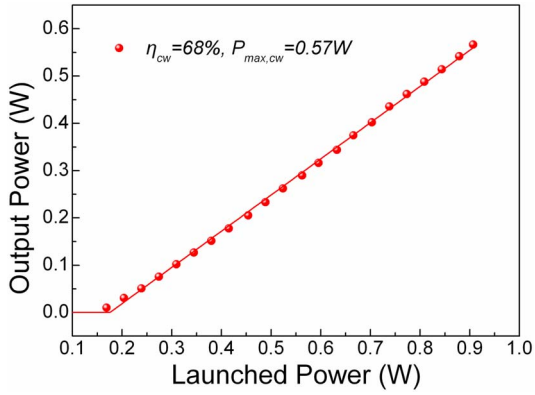

Fig. 2. Output power of cw laser (red line) as a function of the launched power at 808 nm.

was stuck close to the end face of the sample, and the other end face was coated with the thin film mentioned above. With the analysis of the emission spectra of the generated light we confirmed the successful typical laser oscillation from the fs laser inscribed Nd:$GdVO_4$ depressed cladding waveguides, as the absorbed power was above the lasing threshold [Fig. 3(b)]. The central wavelength of the laser emission from the cladding waveguide was placed at 1064.5 nm, which corresponds to the main fluorescence of $^4F_{3/2} \rightarrow {}^4I_{11/2}$ transition in the Nd^{3+} ions, with a FWHM of ~0.6 nm. The inset graph illuminates the typical pulse trains of the passively Q-switched laser under the pump power of 607 mW.

Figure 4 shows the dependence of the pulse duration and the pulse energy as functions of the launched power collected from the Q-switched pulse waveguide laser. The pulse duration and the pulse energy were calculated with the model for Q-switched laser presented in the previous work [28]. When the launched power was near the lasing threshold, i.e., 297 mW, the pulse duration was about 232 ns with the energy of single pulse being 6.6 nJ. In agreement with the theoretical results reported in [29], the pulse duration of the passive Q-switched pulse laser decreased to 75 ns; meanwhile the pulse energy increased to 19 nJ when the launched power was gradually increased to 870 mW.

Figures 5(a) and 3(b) display the 2D laser modal profiles (at 1064.5 nm) in the cw regime at TM and TE polarizations as the launched power was above the threshold at room temperature [Figs. 5(e) and 5(f) are the corresponding 3D plots], and Figs. 5(c) and 5(d) correspond to the modal profiles for pulsed operation [Figs. 5(g) and 5(h) are the 3D plots]. As it has been demonstrated in previous works [8], in the fabrication procedure of the

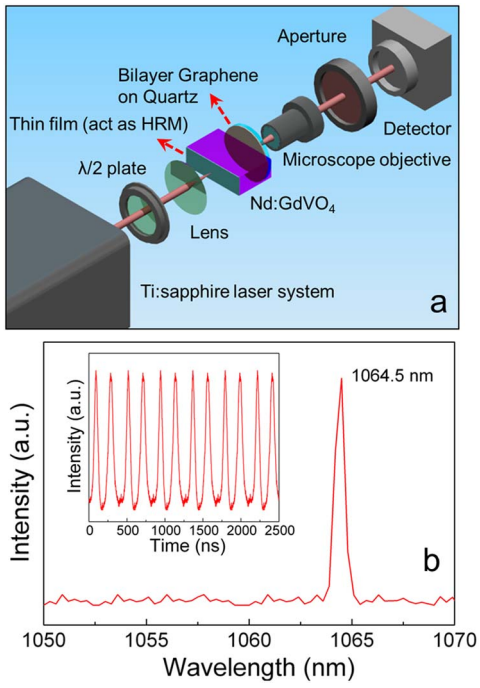

Fig. 3. (a) Experimental setup for the Q-switched waveguide laser measurement and (b) spectrum of cw waveguide laser oscillated at 1064.5 nm (the inset graph is the pulse train of the resonant laser).

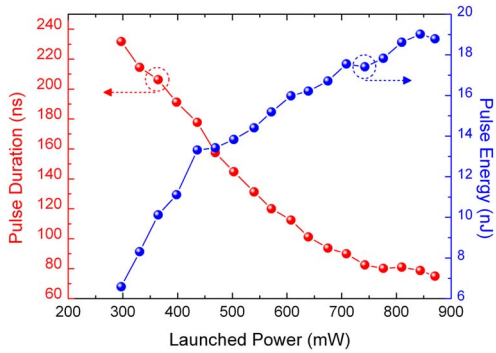

Fig. 4. Efficient graphene Q-switched Nd:$GdVO_4$ waveguide laser at TM polarization: pulse duration (in red spheres) and single-pulse energy (in blue spheres) versus the launched power.

cladding waveguides the stress field induced in the material was relatively more isotropic and symmetric than the highly anisotropic stress filed in double-line waveguides [30]; for this reason the cladding waveguides supported lasing at both TM and TE polarizations with a difference of laser performance less than 10%. It should be pointed out that the TM and TE modes of the waveguide lasers were very similar. In double-line stress-induced Nd:GGG [29], Nd:YAG [8,10], or Ti:sapphire [31] waveguides, guided laser generation was only reported along the TM polarization. In this sense, the cladding waveguide configuration is more advantageous for a pump with nonpolarized diode lasers. According to the previous calculations [32,33], a single-layer graphene owns an efficient absorption coefficient (~2.3%) for the incident visible-to-infrared light, and the modulation depth of pristine monolayer graphene could be up to 65.9%. By considering that the nonsaturable loss increased and the modulation depth of the graphene reduced as a result of the enhancement of layers, the modulation depth of the bilayer graphene could be larger than 30% in this experiment. As one of the typical behaviors in the Q-switched waveguide laser, the calculated repetition rate rises from 5.7 to 17.8 MHz provided that it is proportional to the intracavity intensity and inversely proportional to the pulse duration.

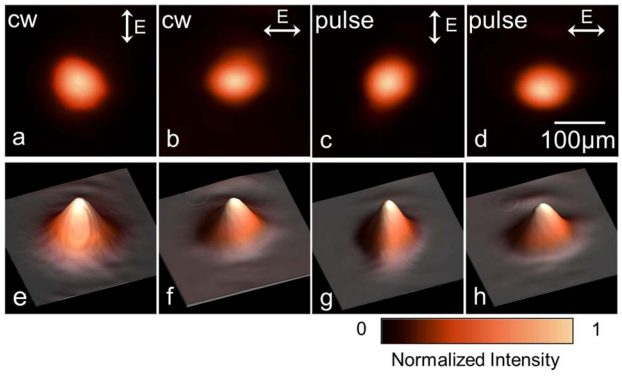

Fig. 5. 2D laser modal profiles of cw lasers at (a) TM and (b) TE polarizations, and profiles of pulsed lasers at (c) TM and (d) TE polarizations when the launched power was above the threshold. (e)–(h) are the corresponding 3D plots.

In conclusion, we have fabricated cladding waveguides in Nd:$GdVO_4$ crystal and realized efficient cw and passively Q-switched waveguide lasing at 1064.5 nm by bilayer graphene SA. Waveguide lasers at both TE and TM polarizations with fundamental modal profiles were achieved. The cw laser was with a maximum output power as high as 0.57 W and a slope efficiency of 68%, which was close to the quantum defect limit. By using the GSA, the passively Q-switched pulse laser was achieved with maximum single-pulse energy of up to 19 nJ. The resonant frequency of 18 MHz was generated with the shortest pulse duration of 75 ns.

The work is supported by the National Natural Science Foundation of China (No. 11274203), the Specialized Research Fund for the Doctoral Program of Higher Education of China (No. 20130131130001), and Junta de Castilla y León under project SA086A12-2. Support from the Centro de Láseres Pulsados (CLPU) is also acknowledged.

References

1. L. Fornasiero, S. Kück, T. Jensen, G. Huber, and B. H. T. Chai, Appl. Phys. B **67**, 549 (1998).
2. V. Ostroumov, T. Jensen, J. P. Meyn, G. Huber, and M. A. Noginov, J. Opt. Soc. Am. B **15**, 1052 (1998).
3. T. Taira, IEEE J. Sel. Top. Quantum Electron. **13**, 798 (2007).
4. K. M. Davis, K. Miura, N. Sugimoto, and K. Hirao, Opt. Lett. **21**, 1729 (1996).
5. F. Chen and J. R. Vázquez de Aldana, Laser Photon. Rev. **8**, 251 (2014).
6. A. G. Okhrimchuk, A. V. Shestakov, I. Khrushchev, and J. Mitchell, Opt. Lett. **30**, 2248 (2005).
7. Y. Ren, J. R. Vázquez de Aldana, F. Chen, and H. Zhang, Opt. Express **21**, 6503 (2013).
8. Y. Jia, J. R. Vázquez de Aldana, Q. Lu, D. Jaque, and F. Chen, Opt. Mater. Express **3**, 1279 (2013).
9. G. Salamu, F. Jipa, M. Zamfirescu, and N. Pavel, Opt. Express **22**, 5177 (2014).
10. N. Pavel, G. Salamu, F. Voicu, F. Jipa, M. Zamfirescu, and T. Dascalu, Laser Phys. Lett. **10**, 095802 (2013).
11. D. G. Lancaster, S. Gross, H. Ebendorff-Heidepriem, K. Kuan, T. M. Monro, M. Ams, A. Fuerbach, and M. J. Withford, Opt. Lett. **36**, 1587 (2011).
12. P. A. Berry, J. R. Macdonald, S. J. Beecher, S. A. McDaniel, K. L. Schepler, and A. K. Kar, Opt. Mater. Express **3**, 1250 (2013).
13. C. Grivas, Prog. Quantum Electron. **35**, 159 (2011).
14. U. Keller, K. J. Weingarten, F. X. Kärtner, D. Kopf, B. Braun, I. D. Jung, R. Fluch, C. Hönninger, N. Matuschek, and J. A. der Au, IEEE J. Sel. Top. Quantum Electron. **2**, 435 (1996).
15. P. T. Guerreiro, S. Ten, N. F. Borrelli, J. Butty, G. E. Jabbour, and N. Peyghambarian, Appl. Phys. Lett. **71**, 1595 (1997).
16. Y. Chen, N. R. Raravikar, L. S. Schadler, P. M. Ajayan, Y. Zhao, T. Lu, G. Wang, and X. Zhang, Appl. Phys. Lett. **81**, 975 (2002).
17. M. N. Cizmeciyan, J. W. Kim, S. Bae, B. H. Hong, F. Rotermund, and A. Sennaroglu, Opt. Lett. **38**, 341 (2013).
18. A. J. DeMaria, D. A. Stetser, and H. Heynau, Appl. Phys. Lett. **8**, 174 (1966).
19. J. Xu, I. J. Thomson, J. D. R. Valera, H. J. Baker, A. B. Russell, and D. R. Hall, IEEE J. Sel. Top. Quantum Electron. **13**, 638 (2007).
20. J. A. Aust, K. J. Malonem, D. L. Veasey, and N. A. Sanford, Opt. Lett. **19**, 1849 (1994).
21. J. W. Kim, S. Y. Choi, D. Yeom, S. Aravazhi, M. Pollnau, U. Griebner, V. Petrov, and F. Rotermund, Opt. Lett. **38**, 5090 (2013).
22. J. I. Mackenzie and D. P. Shepherd, Opt. Lett. **27**, 2161 (2002).
23. S. Balsamo, S. Maio, I. Montrosset, H. Suche, and W. Sohler, Opt. Quantum Electron. **31**, 29 (1999).
24. A. Schmidt, P. Koopmann, G. Huber, P. Fuhrberg, S. Y. Choi, D. Yeom, F. Rotermund, V. Petrov, and U. Griebner, Opt. Express **20**, 5313 (2012).
25. J. Siebenmorgen, T. Calmano, K. Petermann, and G. Huber, Opt. Express **18**, 16035 (2010).
26. R. Ramponi, R. Osellame, and M. Marangoni, Rev. Sci. Instrum. **73**, 1117 (2002).
27. Y. Tan, A. Ródenas, F. Chen, R. R. Thomson, A. K. Kar, D. Jaque, and Q. M. Lu, Opt. Express **18**, 24994 (2010).
28. J. J. Zayhowski and P. L. Kelley, IEEE J. Quantum Electron. **27**, 2220 (1991).
29. C. Zhang, N. N. Dong, J. Yang, F. Chen, J. R. Vázquez de Aldana, and Q. M. Lu, Opt. Express **19**, 12503 (2011).
30. G. A. Torchia, A. Rodenas, A. Benayas, E. Cantelar, L. Roso, and D. Jaque, Appl. Phys. Lett. **92**, 111103 (2008).
31. C. Grivas, C. Corbari, G. Brambilla, and P. G. Lagoudakis, Opt. Lett. **37**, 4630 (2012).
32. Q. Bao, H. Zhang, Y. Wang, Z. Ni, Y. Yan, Z. X. Shen, K. P. Loh, and D. Y. Tang, Adv. Funct. Mater. **19**, 3077 (2009).
33. H. Yu, X. Chen, H. Zhang, X. Xu, X. Hu, Z. Wang, J. Wang, S. Zhuang, and M. Jiang, ACS Nano **4**, 7582 (2010).